Journal of *Marine Science and Engineering*

MDPI

Article

Provenance Analysis of the Northern Offshore Mud Area of the Shandong Peninsula, China, Spanning the Last 2000 Years

Shuyu Wu [1,2,3,4,5], Jun Liu [2,5,*] and Yongcai Feng [2]

[1] School of Engineering, China University of Geoscience (Wuhan), Wuhan 430074, China; hnwushuyu@163.com
[2] Ministry of Natural Resources Observation and Research Station of Land-Sea Interaction Field in the Yellow River Estuary, Yantai Center of Coastal Zone Geological Survey, China Geological Survey, Yantai 264000, China; fyc1107@163.com
[3] Key Laboratory of Submarine Geosciences, Ministry of Natural Resources, Hangzhou 310012, China
[4] Chinese Academy of Geological Sciences, China Geological Survey, Ministry of Natural Resources, Beijing 100037, China
[5] Laboratory for Marine Mineral Resources, Qingdao Marine Science and Technology Center, Qingdao 266237, China
* Correspondence: vnlj@163.com; Tel./Fax: +86-0535-2901607

Abstract: The mud area in the northern offshore of the Shandong Peninsula constitutes a dynamic source–sink system in China's continental shelf and is a hotspot for research. However, the provenance of the sediments remains controversial, and the depositional environment is not yet fully understood. This paper performed accelerator mass spectrometry ^{14}C dating, grain-size analysis, clay mineralogic analysis, and geochemical analysis of the ZZ04 sediment core. The results showed that this core primarily comprises silt and clay, reflecting weak sedimentary hydrodynamic conditions and stable deposition. The clay mineral assemblage—illite, smectite, chlorite, and kaolinite—indicates strong physical weathering. The provenance of the mud area was mainly from the Yellow River, Shandong Peninsula rivers, and Yangtze River, highlighting its multi-source characteristics. The smectite/(illite + chlorite) ratio in the ZZ04 core serves as a mineralogical indicator of the East Asian summer monsoon (EASM). Eight significant East Asian winter monsoon (EAWM) intensifications were identified, correlating with global cooling events similar to those at 1.89, 1.4, 1.03, and 0.62 thousand years ago. During the EAWM period, the coastal current and the Yellow Sea warm current play crucial roles in the transportation of matter and heat flux in the mud area. In contrast, during the EASM period, the sediments are predominantly sourced from the Shandong Peninsula rivers, contributing terrigenous materials shaped by chemical weathering.

Keywords: northern offshore mud area of the Shandong Peninsula; mud area; clay minerals; provenance; East Asian monsoon; Yellow River

Citation: Wu, S.; Liu, J.; Feng, Y. Provenance Analysis of the Northern Offshore Mud Area of the Shandong Peninsula, China, Spanning the Last 2000 Years. *J. Mar. Sci. Eng.* **2024**, *12*, 1501. https://doi.org/10.3390/jmse12091501

Academic Editors: Anabela Oliveira and Gemma Aiello

Received: 5 July 2024
Revised: 28 August 2024
Accepted: 29 August 2024
Published: 1 September 2024

1. Introduction

The East China shelf marginal sea emerged during the Holocene high-sea-level period, and its sedimentary processes are influenced by the East Asian monsoon. Global sea level fluctuations have led to the formation of several patchy mud areas, which are primarily sourced from sediments carried by major rivers such as the Yellow River (YR) and the Yangtze River. The circulation system, driven by warm and coastal currents, is crucial for sediment transport and deposition [1]. Seven mud areas have been identified on the eastern shelf of China, including the central Bohai Sea (BS) mud area [2], the northern offshore mud area of the Shandong Peninsula [3–6], the eastern Yellow Sea (YS) mud area [7], the central South Yellow Sea (SYS) mud area [8,9], the inland shelf mud area of the East China Sea (ECS) [10,11], the Jeju island mud area [12], and the Beibu Gulf of the South China Sea (SCS) mud area [13]. The northern offshore mud area of the Shandong Peninsula is a significant focus for oceanographic research owing to its rapid

sedimentation rates coupled with organic matter burial capabilities and unique geological and geographical attributes [6,14–16]. In the 1980s, Milliman et al. [3] identified an Ω-type subaqueous delta, known as the "Shandong Peninsula mud wedge" [4,17], which has an evolutionary history closely tied to sedimentation from the YR and the Yangtze River. This area provides a detailed record of marine environment changes, including sea level fluctuations, shelf circulation patterns, monsoon evolution, hydrodynamic environment changes, and sediment transport and deposition processes [6,14–16]. Moreover, it serves as an ideal location for studying sediment source–sink dynamics and ocean–land interactions.

Numerous scholars have conducted extensive research on the provenance of the mud area of the Shandong Peninsula. For instance, Wang et al. [18] analyzed the grain-size characteristics of surface sediments in the North Yellow Sea (NYS), reporting that grain-size distribution is primarily influenced by the provenance and sedimentary environment with a significant impact from coastal currents, particularly in the mud area's extension from southwest to northeast. Chen et al. [19] examined the geochemistry of surface sediments in the western part of the NYS, concluding that sediments from the YR are the main source of this region' s sedimentary deposits. Based on ^{210}Pb dating of core sediments, Qi et al. [20] revealed that the western part of the NYS is a multi-source sedimentary area, with YR sediment as the primary source. Liu et al. [21] investigated the sediment provenance in the western part of the NYS since the last glacial maximum using rare-earth elements from the NYS101 borehole sediments. They highlighted that since the Middle Holocene, in addition to the YR sediment, sediments from the Yangtze River and Korean Peninsula rivers have influenced this region. Lan et al. [22] analyzed the major and trace elements of the DLC70-2 borehole sediments, revealing that since the early Late Pleistocene, the YR has been the primary provenance, and the Yalu River exerts a significant influence in the NYS. Xue et al. [6] suggested that the Shandong Peninsula's mud area, rather than forming concurrently with the YR delta, is actually a large mudflat–tidal delta on the seaward side of the Bohai Strait. Furthermore, analyzing the geochemical and clay mineral characteristics of the mud area in the middle of the NYS, Han et al. [23] concluded that the NYS is a multi-source sedimentary area. Its provenance included not only the YR sediments transported by the Shandong coastal current, but also the Liaodong Peninsula river sediments and the Yangtze River sediments carried by the Yellow Sea warm current (YSWC) and atmospheric dust.

Clay minerals serve as a distinctive "fingerprint" for fine-grained sediments of different origins. Owing to their ability to be transported before settling, clay minerals can reveal the sediment source. By analyzing the clay mineralogy of sediments, the transport pathways of suspended matter can be traced. Moreover, the assemblages of clay minerals are intimately connected with the sediment's provenance and climatic evolution, making them a useful tool for reconstructing paleoclimatic and paleoceanographic conditions [24–26]. Given the varied bedrock types and climates across regions, such as the Shandong Peninsula, the Korean Peninsula, and the YR, establishing a correlation between the specific clay mineral assemblages, their sources, and the patterns of their circulation is possible. Monitoring the changes in these assemblages provides a valuable indicator for assessing sedimentary environments and identifying the origins of source materials.

However, the provenance of the sediments of this area remains controversial, and the depositional environment is not yet fully understood. In this study, we utilized a newly acquired core sample, ZZ04, to construct a dating framework using accelerator mass spectrometry (AMS) ^{14}C. Using this framework as a foundation, we conducted grain-size and clay mineral analyses. The study aimed to (1) elucidate the clay mineral assemblages in the mud area and its surroundings, (2) ascertain the provenance of the sediments in the mud area, and (3) investigate the influence of climate change and provenance on the mud area's sedimentary features at different periods.

2. Geological Setting

The NYS is a semi-enclosed marginal sea situated in the Liaodong Peninsula to the northwest, the Shandong Peninsula to the south, and the Korean Peninsula to the east. Its geographical location is approximately between 121°00′ E to 125°10′ E longitude and 37°20′ N to 39°50′ N latitude (Figure 1a). Resembling a half-graben-shaped depression, it opens to the southeast and is characteristic of a typical shallow continental shelf environment [27]. The NYS has an average water depth of 38 m, with the deepest points reaching up to 80 m. It features a shallow plain in the north, where the seabed topography gradually inclines toward the south, and a relatively deep central depression [28].

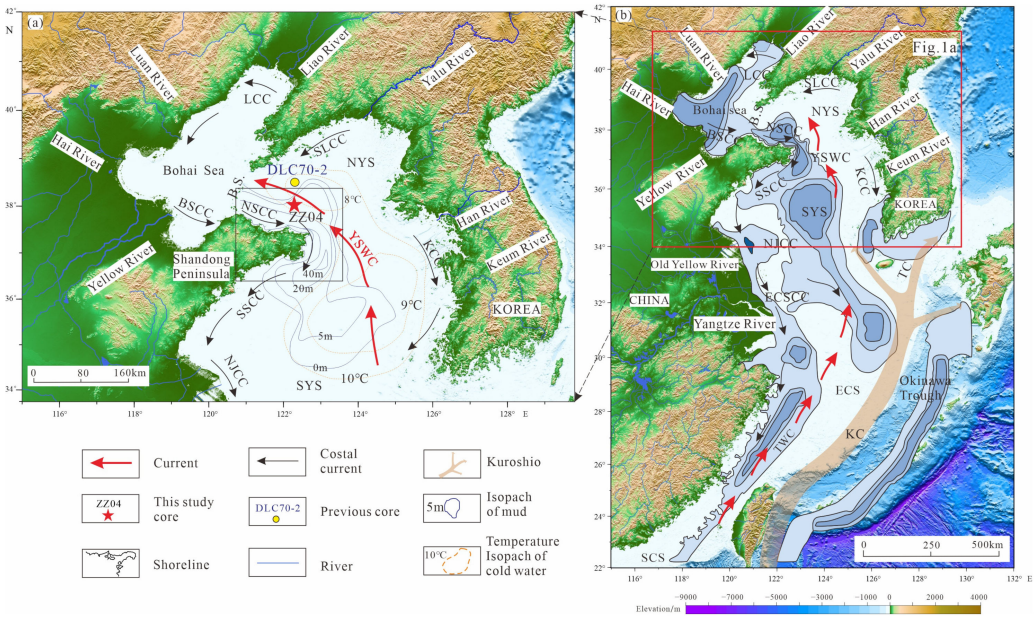

Figure 1. Sketch map showing the oceanographic settings and core location. (**a**) Regional circulation patterns in the Yellow Sea and the Bohai Sea. (**b**) Sketch map showing the circulation patterns in China's eastern marginal sea and the distribution of mud areas. Coastal circulation is indicated by the black arrows, while warm circulation is indicated by the red arrows. The study area is enclosed by the red rectangle. The main currents include the South Liaoning coastal current (SLCC), Liaoning coastal current (LCC), Bohai Sea coastal current (BSCC), North Shandong Peninsula coastal current (NSCC), South Shandong Peninsula coastal current (SSCC), North Jiangsu coastal current (NJCC), Korean coastal current (KCC), East China Sea coastal current (ECSCC), Yellow Sea warm current (YSWC), Taiwan warm current (TWC), and Kuroshio current (KC). The geographical abbreviations include the Bohai Strait (B.S.), North Yellow Sea (NYS), South Yellow Sea (SYS), East China Sea (ECS), and South China Sea (SCS). The main cores studied in this paper are ZZ04 (this study) and a previous study core, DLC70-2 [22].

The basement comprises mainly Archean–Lower Proterozoic metamorphic rocks and Middle and Upper Proterozoic–Cambrian carbonate rocks and slate. From the Middle Jurassic, the basin began to subside, and the sedimentary succession is composed of Middle–Upper Jurassic, Lower Cretaceous, Eocene, Oligocene, and Neogene–Quaternary sediments with terrigenous clastic rock [29]. The NYS receives sediments from several major rivers, including the YR, Yalu River, Korean Peninsula rivers, Shandong Peninsula rivers, and Yangtze River. The YR, with a length of 5463 km, has an average annual runoff of 42.6×10^9 m^3 and transports a sediment discharge of 1089 Mt/year. The Yalu River, with a length of 790 km, has an average annual runoff of 28.9×10^9 m^3 and transports a sediment discharge of 1.13 Mt/year. Approximately 417 km in length, the Han River flows into the SYS in Gyeonggi Province, South Korea. It has an average annual runoff of approximately 19×10^9 m^3 and transports a sediment discharge of approximately 1.84 Mt/year [30].

As a branch of the Kuroshio current (KC), the YSWC flows northwest into the SYS, continuing its journey into the NYS. It extends through the northern part of the Bohai Strait, further reaching into the BS [31,32] (Figure 1b). The YSWC is vigorous in winter yet relatively weak in summer [5,33]. The Shandong coastal current originates from the Bohai Bay, moving eastward along the northern coast of the Shandong Peninsula. Then, it turns southwest at Chengshan Head, following the 40–50 m isobath until it veers south near Laoshan Bay, Qingdao. This coastal current converges with the northbound YSWC, creating a cyclonic circulation system. The path of the Shandong coastal current remains largely stable throughout the year. Near the Chengshan Head, the flow narrows and accelerates to 15 cm/s, peaking at 110 cm/s. The bottom coastal current in the YS is similar to that in the surface layer, albeit with a lower velocity and a more shoreline–proximate flow path [27].

3. Materials and Methods

3.1. Sample Collection

The study samples originated from the ZZ04 core, which was collected by the Yantai Center of Coastal Zone Geological Survey (YCGS) from the northern offshore area of the Shandong Peninsula in 2023 (Figure 1a). The sample site is located at 37.963203° N and 122.370869° E, with a water depth of 44.2 m and a total core length of 3.3 m. The core's lithology primarily comprised gray silty clay and clayey silt.

To ensure the consistency between the river data from the references and our test results, five samples from the YR estuary were collected for concurrent analyses. After collection, these core samples were cut into 2 cm thick sections. Grain-size analysis was conducted at 2 cm intervals, resulting in 163 samples, whereas clay mineralogic and geochemical analyses were performed at 4 cm intervals, resulting in 71 samples, respectively.

3.2. AMS ^{14}C Dating

To establish a dating framework for this core, two samples containing benthic foraminifera were selected and subjected to AMS ^{14}C dating conducted at the Institute of Hydrogeology and Environmental Geology, Chinese Academy of Geological Sciences (Shijiazhuang city, China). The procedure mainly involved three steps. First, the carbon in the sample was converted to CO_2 through combustion. Then, CO_2 was reduced to graphite using a zinc and iron catalyst. Lastly, the sample's age was calculated based on the ^{14}C ratio. The AMS ^{14}C age-dating process was facilitated by a Zn/Fe flame-sealed tube AMS (0.5MV 1.5SDH-1 model, NEC Corporation, Irving, TX, USA), which maintains a long-term $^{14}C/^{12}C$ testing accuracy of higher than 3%. The instrument's background value was Fm = 0.0004, which is equivalent to 63,764 years.

For samples calibrated in the NYS, a correction value of $\Delta R = -276 \pm 52$ years was applied [34]. The ^{14}C age was then calibrated to a calendar age (cal.a B.P., relative to 1950 CE) using the CALIB 7.0.2 software [35].

3.3. Grain-Size Analysis

Grain-size analysis was performed at the YCGS Testing Center using the PSA 1190LD laser grain-size analyzer (Anton Paar, Ashland, VA, USA). This instrument has a measurement range of 0.98–2500 μm and ensures a relative error of less than 1% for repeated measurements. Briefly, after adding 0.1 mol/L HCl to the samples to remove carbonate and 10% H_2O_2 to eliminate organic materials, 0.5 mol/L $Na(PO_3)_6$ was added and thoroughly mixed. Then, the samples were diluted to an appropriate concentration after removing the supernatant and allowing the samples to stand for 24 h. Prior to measurement, additional disaggregation was carried out using an ultrasonic cleaner for 1 min. Parameters, including the mean particle size, sorting coefficient, skewness, and kurtosis, of the sediment fractions were calculated using Folk's method [36].

3.4. Clay Mineralogic Analysis

Clay mineralogic analysis was performed at the Qingdao Sibada Company using the Bruker D8 X Ray diffractometer (Bruker AXS, Karlsruhe, Germany). First, the sample was placed in a 50 mL centrifuge tube and immersed in 10% H_2O_2 to remove organic material. Residual H_2O_2 was neutralized by adding pure water, followed by centrifugation at 3500 rpm. Next, 50% glacial acetic acid was added to the sample to remove carbonate minerals. Then, it was centrifuged and washed with water several times until it reached a neutral pH. The suspended particles of the upper clay fraction (less than 2 μm) were transferred to a new centrifuge tube containing two drops of 26% saturated NaCl. After centrifugation, the supernatant was extracted and used to prepare a slide. The slide was allowed to air-dry naturally before being placed in a dryer containing ethylene glycol at the bottom. It was then baked at 60 °C for 6 h prior to X-ray diffraction (XRD) testing.

Each sample underwent three evaluations: (1) In dry air conditions, a Δ2θ scan was performed from 3° to 30.1°, with a step size of 0.021°. (2) Under ethylene glycol saturation, a Δ2θ scan was conducted from 3° to 30.1° with the same step size. (3) Under ethylene glycol saturation, a Δ2θ scan was performed from 24° to 26°, with a smaller step size of 0.011°. Additionally, some of the ethylene glycol saturation samples were heated at 550 °C for 2 h to further identify kaolinite and chlorite and to confirm the presence of smectite.

In the analysis of clay minerals, we employed the Al_2O_3 standard spectrum as a benchmark. The relative abundances of the clay minerals were determined according to Biscay's method [37], and the ethylene glycol saturation curves were drawn using the Jade 7.5 software. The diffraction peak areas for smectite (17 Å), illite (10 Å), and kaolinite–chlorite (7 Å) were multiplied by their respective intensity factors of 1, 4, and 2. The proportion of chlorite to kaolinite was derived from their diffraction peak areas at 3.54 Å and 3.58 Å. These characteristic peak areas of the four clay minerals were normalized to a total of 100%.

The illite chemical index (ratio of the 5 Å to 10 Å peak areas in the glycolated curve) is often used as an intuitive indicator of provenance characteristics [38,39]. According to Esquevin's classification [40], illite is considered Fe-Mg rich when its chemical index is less than 0.5, indicating strong physical weathering. Conversely, an index greater than 0.5 suggests Al-rich illite, reflecting strong chemical weathering [41,42]. The 10Å FWHM is defined as the full width at half-maximum of the 10Å mica peak.

Cluster analysis is an unsupervised learning method that reveals the intrinsic structure and patterns of data by grouping similar data points into clusters. In source classification, cluster analysis can be used to identify and differentiate various data, thereby providing a basis for the source tracer [43]. In this paper, we used the ternary diagram and crossplot methodologies to achieve these analytical objectives.

3.5. Geochemical Analysis

Major and trace element analysis was conducted at the YCGS Testing Center using the Axios X fluorescence spectrometer (Panaco Company, Almelo, The Netherlands). Samples were initially dried, pelletized, and digested using a mixture of 4 mL nitric acid (HNO_3) and 1 mL perchloric acid ($HClO_4$), followed by a mixture of 4 mL hydrofluoric acid (HF) and 1 mL perchloric acid ($HClO_4$). The procedure was completed by adding 10 mL of nitric acid (HNO_3).

X-ray fluorescence spectroscopy was utilized to measure the concentration of major elements, including Si, Al, Ca, Mg, K, and Na, and trace elements, including Cu, Pb, Zn, Cr, Ni, Co, Cd, Rb, Sr, and Ba. The MgO/Al_2O_3 ratio in marine sediments indicates the extent of terrigenous material input but does not account for grain-size effects in regions where terrigenous clastic materials predominate. Generally, a higher MgO/Al_2O_3 ratio indicates a lower terrigenous material input [44]. Changes in the Sr/Ca ratio serve as an indicator of the biological activity of phytoplankton in the marine surface waters. As microscopic plants grow, they incorporate calcium ions (Ca^{2+}) into their skeletal structures while taking up comparatively lower amounts of strontium ions (Sr^{2+}). Given the chemical similarities between Sr^{2+} and Ca^{2+}, their competitive uptake can establish a correlation between the

Sr/Ca ratio and the level of marine productivity. An elevated productivity signifies a higher absorption of Ca^{2+} by the organisms, which subsequently leads to a decreased Sr/Ca ratio. During periods of lower productivity, the Sr/Ca ratio is relatively higher, reflecting less competition for calcium during phytoplankton growth [45].

4. Results

4.1. Grain-Size Analysis

The lithology of core ZZ04 predominantly consisted of gray clayey silt and silty clay (Figure 2a). The sediments were primarily composed of silt (4–63 μm), clay (<4 μm), and sand (>63 μm), whose contents ranged from 75.7–81.09% (average: 77.94%, Figure 2b), 17.88–24.19% (averaged 21.64%, Figure 2c) and <1.5% (Figure 2d), respectively. The sediments primarily consisted of silt, according to the Shepard classification (Figure 3a). The grain-size curves indicated a clear stratification into two sections at a depth of 1.83 m (~1.63 cal.ka B.P.).

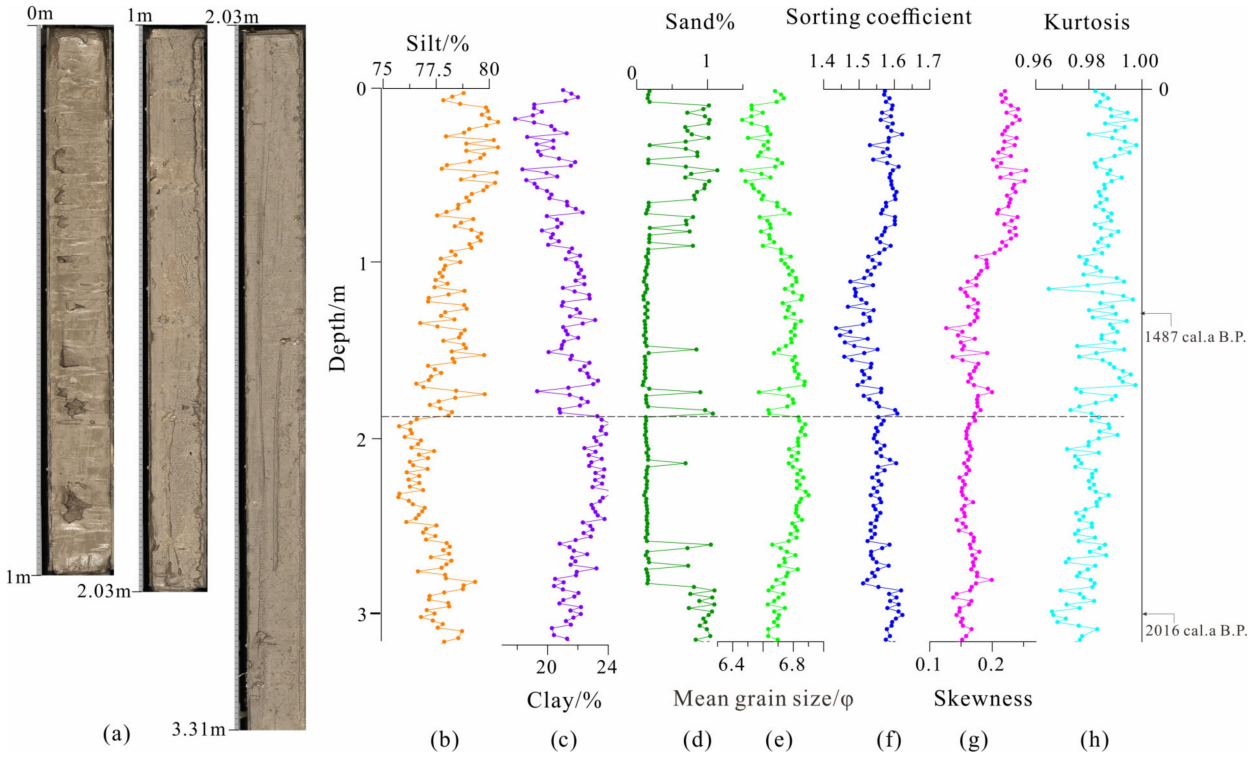

Figure 2. Sediment grain-size curves in the ZZ04 core. From left to right: (**a**) photographs of the cores, (**b**) silt content (4–63 μm), (**c**) clay content (<4 μm), (**d**) sand content (>63 μm), (**e**) mean particle size, (**f**) sorting coefficient, (**g**) skewness, and (**h**) kurtosis. Black arrows show the calendar ASM ^{14}C-age of the benthic foraminifera.

In the lower section (1.83–3.37 m), from the bottom to the top depth, the silt content decreased, and the clay content increased (Figure 2b,c). The mean particle size slightly increased from 6.63 Φ to 6.87 Φ, indicating a transition from coarser to finer sediments (Figure 2e). The sorting coefficient and skewness curves exhibited minor fluctuations around 1.55 and 0.15, respectively, suggesting a moderate sorting degree and a positive bias distribution (Figure 2f,g). The kurtosis showed a medium level and an overall upward trend from 0.96 to 0.99 (Figure 2h).

In the upper section (0–1.83 m), there was a transition from finer to coarser sediments. As the primary component, the silt content increased from 76% to 81% (Figure 2b). Concurrently, the clay content decreased from 22% to 18% (Figure 2c), whereas the sand content remained minimal, fluctuating between 0 and 1% (Figure 2d). The mean particle size

showed moderate decreases from 6.87 Φ to 6.46 Φ (Figure 2e). The sorting coefficient initially decreased and then increased, indicating a medium sorting level (Figure 2f). Skewness was stable below 1 m, with a value of 0.15, then began to rise above 1 m, showing an overall positive bias (Figure 2g). The kurtosis fluctuated at approximately 0.9, indicating a medium level (Figure 2h).

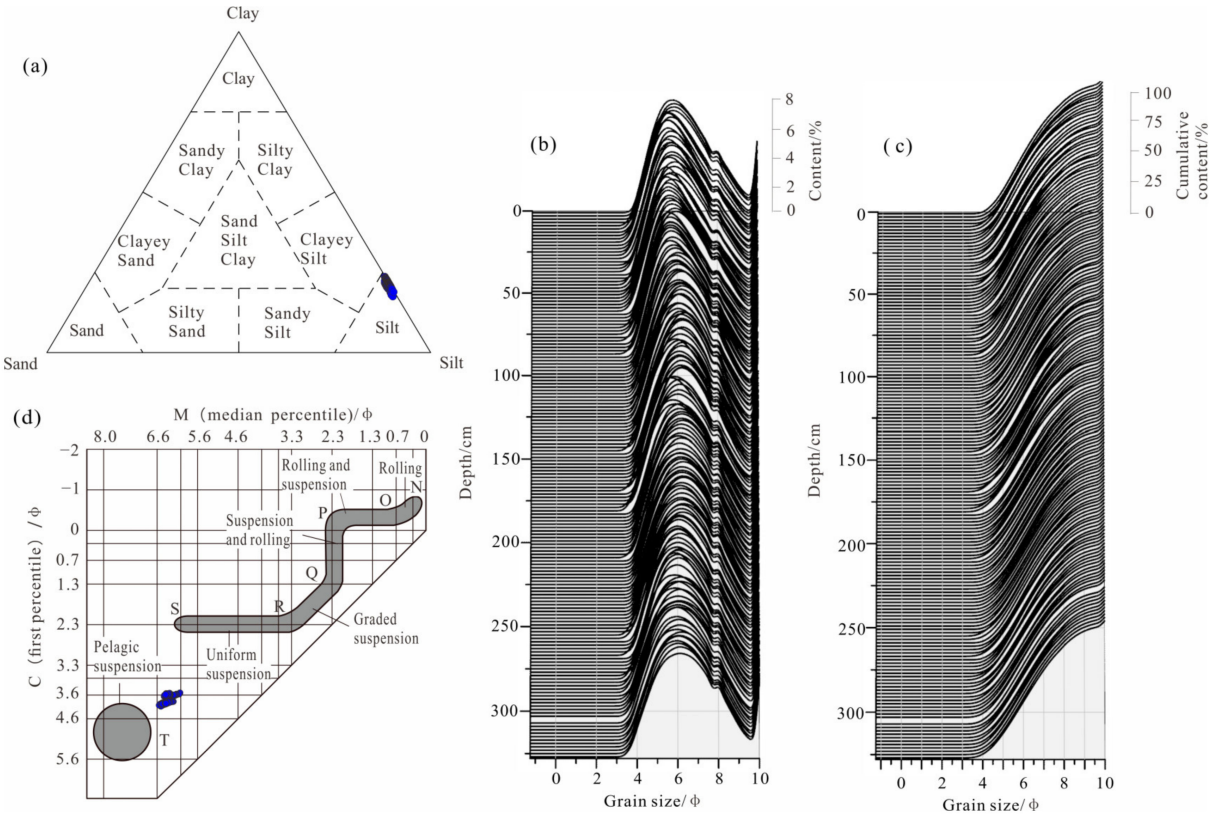

Figure 3. Characteristics of sediment grain-size of core ZZ04. (**a**) Lithology ternary diagrams based on the Shepard classification. (**b**) Grain-size distribution, (**c**) grain-size probability distribution, and (**d**) C-M diagrams.

The grain-size distribution of the ZZ04 core showed a unimodal pattern, with the main peak mode between 5Φ and 6Φ, suggesting a relatively singular provenance (Figure 3b). The grain-size probability curve showed a two-stage distribution, highlighting the predominance of suspension components and scarcity of saltation components (Figure 3c). The C-M diagram showed a sedimentation mode between marine and uniform suspensions, implying weak sedimentary hydrodynamic conditions (Figure 3d).

4.2. Sediment Chronology

The AMS ^{14}C dating results are presented in Table 1 and Figure 2. The age of each sampling interval was established by linear interpolation.

Table 1. AMS ^{14}C and calendar ages of core ZZ04.

Sample ID	Depth (cm)	Material	AMS^{14} C Age (a B.P.)	Calendar Age (cal.a B.P.)	1σ Error Range (cal.a B.P.)
ZZ04-135	134	Mixed benthic foraminifera	1810 ± 35	1487	1385–1576
ZZ04-315	314	Mixed benthic foraminifera	2250 ± 30	2016	1911–2119

The ZZ04 samples collected in 2023 indicated a calendar age of −73 cal.a B.P. at 0 m. The linear sedimentation rates (LSRs) of the sediment layer showed a lower mean value

(0.086 cm/a) above 134 cm and a higher mean value (0.34 cm/a) between 134 cm and 314 cm. Moreover, the ZZ04 core sediments covered a time span of −73 to 2050 cal.a B.P., providing a continuous sediment record.

4.3. Clay Minerals

The XRD pattern of core ZZ04 revealed that it was predominantly composed of clay minerals, including illite, smectite, chlorite, and kaolinite. Additionally, the sample contained some clastic minerals, such as quartz and feldspar (Figure 4).

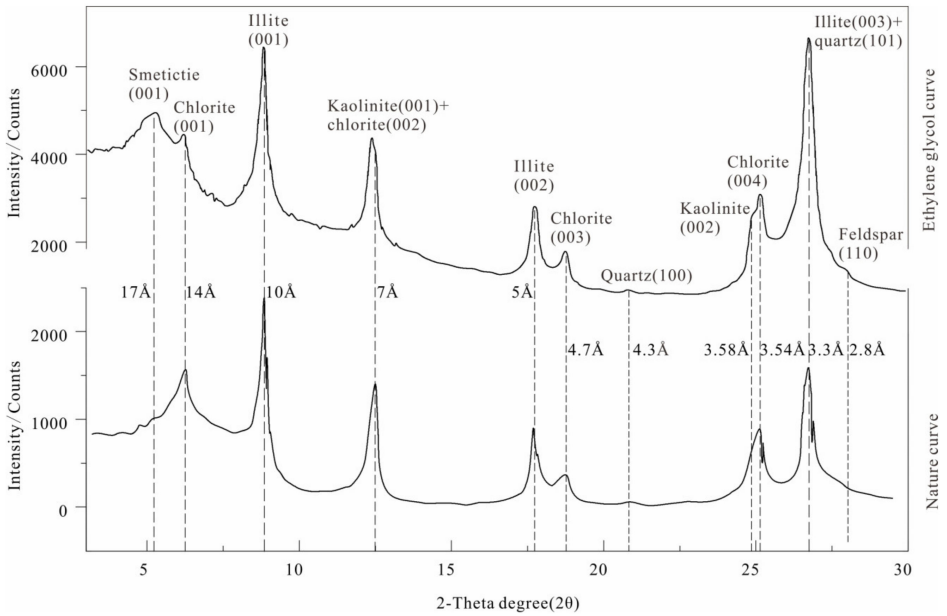

Figure 4. Ethylene glycol curves (up) and natural curves (down) of the X-ray diffraction of clay minerals from core ZZ04.

The clay minerals in core ZZ04 were primarily composed of illite, smectite, chlorite, and kaolinite, whose content ranged from 52.93–69.78% (average: 62.1%, Figure 5a), 12.78–26.4% (average: 18.11%, Figure 5b), 7.95–16.53% (average: 11.7%, Figure 5c), and 5.27–10.39% (average: 7.9%, Figure 5d), respectively. The clay mineral assemblage was illite–smectite–chlorite–kaolinite. The distribution pattern of the clay mineral assemblage revealed a stratification into two sections at a depth of 1.83 m. The clay mineral content remained relatively stable in the lower section. However, the smectite content exhibited a declining trend. Meanwhile, in the upper section, the illite content increased, whereas the chlorite content decreased (Figure 5a,d). The kaolinite content showed a positive correlation with that of chlorite (with a correlation coefficient of 0.66). In contrast, there was a negative correlation between the contents of kaolinite and illite (correlation coefficient of −0.65; Table 2).

Table 2. Correlation analysis of the clay minerals.

	Illite	Smectite	Chlorite	Kaolinte
Illite	1	−0.722	−0.602	−0.650
Smectite	−0.722	1	−0.071	0.068
Chlorite	−0.602	−0.071	1	0.660
Kaolinte	−0.650	0.068	0.660	1

In the ZZ04 core, the 10Å FWHM ranged from 0.2° to 0.32° (2θ), with an average of 0.24° (2θ) (Figure 5e). The illite chemical index in the core ZZ04 samples varied from

0.23–0.47 (average: 0.34), placing it between Fe-Mg types. This is indicative of strong physical weathering (Figure 5f).

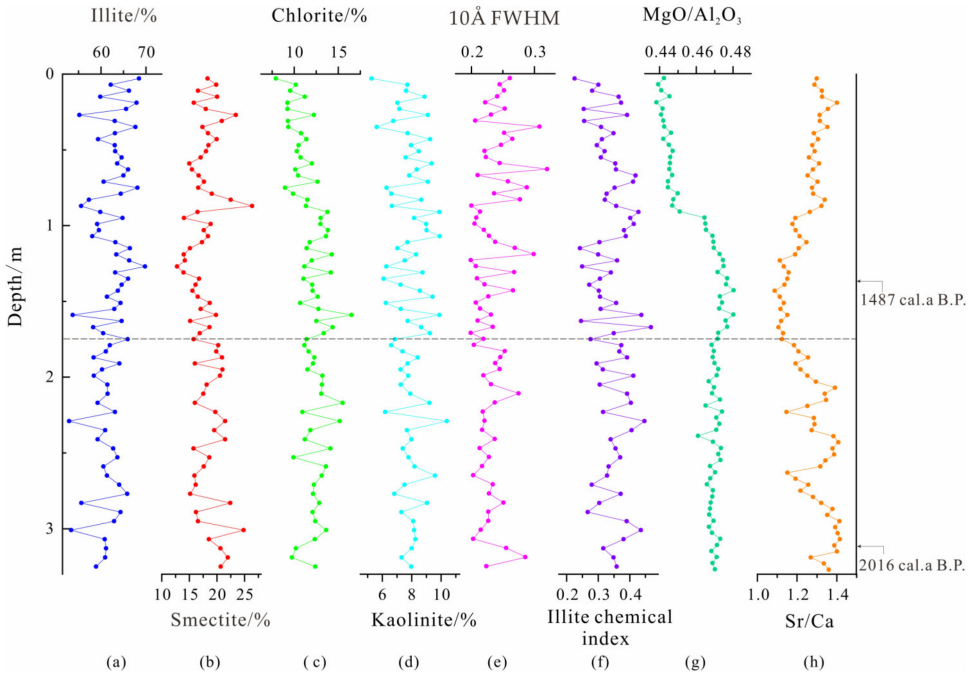

Figure 5. Clay mineral and geochemical curves of core ZZ04. (**a**) Illite content, (**b**) smectite content, (**c**) chlorite content, (**d**) kaolinite content, (**e**) 10Å FWHM, (**f**) illite chemical index, (**g**) MgO/Al_2O_3 ratio, and (**h**) Sr/Ca ratio. Black arrows show the calendar ASM ^{14}C age of the benthic foraminifera.

4.4. MgO/Al_2O_3 and Sr/Ca Ratios

The MgO/Al_2O_3 ratio ranged between 0.44 and 0.48, with an average value of 0.46. Below 0.95 m, this ratio remained stable, averaging approximately 0.47. Above 0.95 m, the ratio had a lower value of 0.44 (Figure 5g).

The Sr/Ca ratio ranged from 1.09 to 1.42, with an average value of 1.27. In the lower section (1.83–3.37 m), the Sr/Ca ratio decreased from 1.4 to 1.1, whereas in the upper section (0–1.83 m), it increased from 1.1 to 1.4 (Figure 5h).

5. Discussion

5.1. Provenance Identification of the Mud Area

The clay minerals in this area predominantly originated from a terrestrial source. These minerals were transported and deposited by the surrounding rivers [46,47]. The NYS receives inputs potentially from the YR, Yangtze River, Yalu River, Shandong Peninsula rivers, and Korean Peninsula rivers (including the Han, Keum, and Yeongsan rivers). A comparative analysis of the clay mineral composition from these rivers enables an examination of how sediments from various rivers influence the distribution patterns of clay minerals (Table 3, Figure 6).

The sediments transported by the YR are largely influenced by the characteristics of the Loess Plateau. The loess is predominantly composed of evaporites and carbonates and has an alkaline-to-weakly-alkaline pH. The YR basin is in a cold and dry climate and is strongly affected by physical weathering processes. The clay mineral compositions reported in the references and those from our results were consistent, which attests to the reliability of the test outcomes. The YR's clay minerals were notably high in smectite (12–23%) and relatively low in kaolinite (8–13%). Additionally, the illite/smectite ratio was less than 6 (Table 3) [2,48–54].

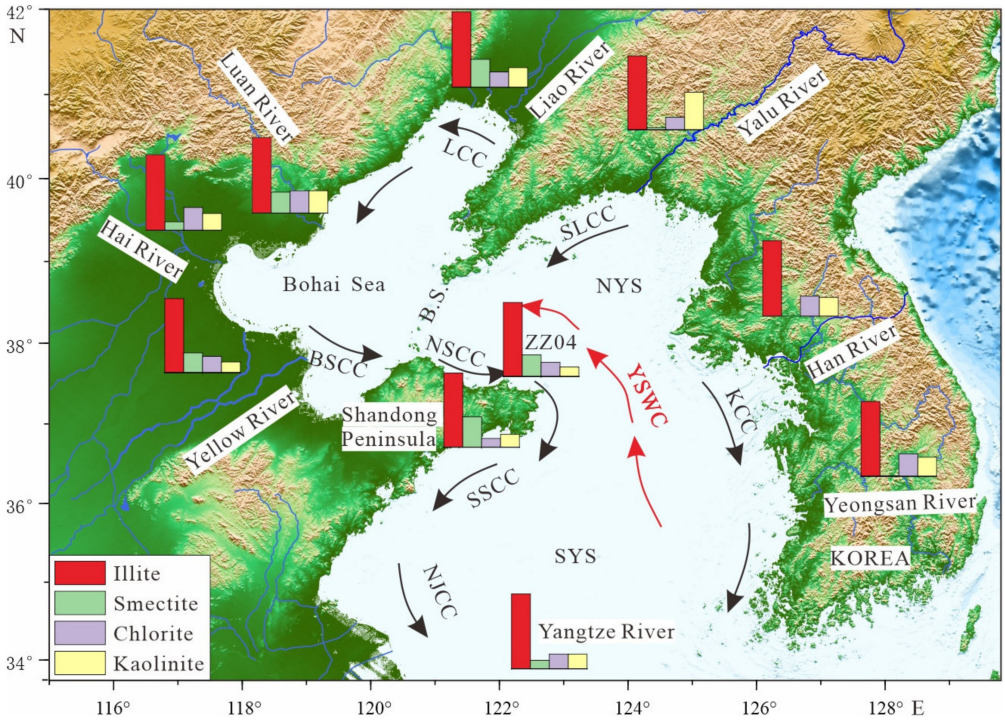

Figure 6. Diagram of the clay mineral composition in the study area and around the YS and BS. The main currents include the South Liaoning coastal current (SLCC), Liaoning coastal current (LCC), Bohai Sea coastal current (BSCC), North Shandong Peninsula coastal current (NSCC), South Shandong Peninsula coastal current (SSCC), North Jiangsu coastal current (NJCC), Korean coastal current (KCC), and Yellow Sea warm current (YSWC). Geographical abbreviations include the Bohai strait (B.S.), North Yellow Sea (NYS), South Yellow Sea (SYS), and East China Sea (ECS).

The Yangtze River's drainage spans the South China orogenic belt, the Yangtze platform, the Qinling–Dabie Mountain orogenic belt, and the Sanjiang Paleo-Tethys orogenic belt. The river's drainage area contains extensive areas of carbonate rocks and terrigenous clastic rocks, with a significant presence of medium-acid intrusive rocks, schists, and gneiss [39,50]. The Yangtze River basin is in a warm and humid climate, and the soil is mostly weakly acidic to acidic, and the chemical weathering is stronger than that in the YR basin [39,50]. The clay mineral assemblage indicates moderate levels of kaolinite at approximately from 8–15%, low levels of smectite ranging from 2–10%, and an illite/smectite ratio exceeding 8 (Table 3) [48,53,55–57].

The Shandong Peninsula's surface is characterized by exposure to Precambrian metamorphic rocks and Yanshanian granite [47]. The composition of clay minerals in this regional river resembles that in the YR; however, the smectite content is notably higher (20–25%) (Table 3) [47,58], which is likely attributed to the extensive weathering of basic volcanic rocks [59].

The Korean Peninsula rivers—the Han, Keum, and Yeongsan rivers—are situated in the Yangtze Plate and are mainly composed of Precambrian gneiss, Jurassic and Cretaceous granites, and Quaternary loose alluvial deposits [32,59–61]. Carbonate outcrops are scarce, with the Jurassic Daebo granite and Late Cretaceous Bulguksa granite as the primary source rocks for the Keum and Yeongsan Rivers, respectively [60]. Such geological conditions can increase the contents of illite, chlorite, and kaolinite while hindering the development of smectite, resulting in a relatively low smectite content (typically less than 2%) (Table 3) [52,62–66].

Situated within the Sino-Korean Plate, the Yalu River predominantly consists of metamorphic rocks, such as amphibole, granulite, and biotite gneiss, along with various pyroxenite groups. The developed rock joints and fissures lead to pronounced spherical

and network weathering patterns [67]. The distribution of clay minerals in the Yalu River is similar to that in the Korean Peninsula rivers, which favors the formation of illite and kaolinite but not that of smectite (whose content is typically below 2%) (Table 3) [52,61].

The ZZ04 core showed a clay mineral assemblage comprising illite, smectite, chlorite, and kaolinite. The relatively high smectite content (average value is 18%, Table 3) suggests a substantial influence from the YR materials. By contrast, the relatively low kaolinite content (average value is 8%, Table 3) indicates that physical weathering predominantly affected this study area. Based on this analysis, the composition of the clay minerals in core ZZ04 is similar to that of the YR and Shandong Peninsula rivers.

Table 3. Clay mineral assemblages and their relative content of river sediments around the NYS.

Rivers	Illite/%	Smectite/%	Chlorite/%	Kaolinite/%	References
Yellow River	61	21	9	9	Liu et al., 2010 [2]
	63	15	13	10	Fan et al., 2001 [48]
	65	14	12	9	Milliman et al., 1985 [49]
	56	21	13	10	Xu et al., 2009 [50]
	59	23	9	9	Xu, 1985 [51]
	67	13	12	8	Ren, 1986 [52]
	62	16	12	10	Yang, 1988 [53]
	62	12	16	10	Yang et al., 2003 [54]
	60	10	18	12	Yang et al., 2003 [54]
	55	13	18	13	This paper
	60	15	13	11	This paper
	56	17	16	11	This paper
	57	17	15	11	This paper
	64	13	14	9	This paper
Yangtze River	71	7	13	9	Fan et al., 2001 [48]
	65	10	11	14	Yang, 1988 [53]
	66	2	17	15	He et al., 2013 [55]
	68	6	14	13	Xu, 1983 [56]
	71	7	14	8	Lu et al., 2015 [57]
Shandong Peninsula rivers	58	25	10	8	Liu et al., 2022 [47]
	58	24	7	11	Liu et al., 2022 [47]
	59	24	7	10	Liu et al., 2022 [47]
	64	19	9	8	Liu et al., 2022 [47]
	57	12	15	16	Hu et al., 2018 [58]
Han River	57	0	23	20	Park et al., 1991 [62]
	70	1	13	17	Park et al., 1992 [63]
	60	2	21	17	Cho et al., 2015 [64]
Keum River	59	1	10	30	Ren et al., 1986 [52]
	55	1	24	21	Cho et al., 2015 [64]
	64	0	17	19	Choi, 1981 [65]
Yeongsan River	64	2	20	15	Cho et al., 2015 [64]
	64	0	19	17	Kim, 1980 [66]
Yalu River	59	1	10	30	Ren et al., 1986 [52]
	68	2	12	18	Yang et al., 2003 [61]
Average of Yellow River (N = 14)	60	16	14	10	
Average of Yangtze River (N = 5)	68	6	14	12	
Average of Shandong Peninsula rivers (N = 5)	59	21	10	11	
Average of Han River (N = 3)	62	1	19	18	
Average of Keum River (N = 3)	59	1	17	23	
Average of Yeongsan River (N = 2)	64	1	19	16	
Average of Yalu River (N = 2)	64	2	11	24	
Average of core ZZ04 (N = 71)	62	18	12	8	

The analysis of clay minerals present in the surface sediments indicates that this study area arose mainly from the YR's sediments. We applied cluster analysis to the ZZ04 core and to samples from adjacent rivers to further elucidate the provenance of the mud area in the Shandong Peninsula. This analysis included a ternary clay mineral diagram (smectite–chlorite–illite + kaolinite; Figure 7a) and a crossplot (illite/smectite and chlorite/kaolinite ratios, Figure 7b). In addition, the clay mineral of the core DLC70-2 in the northern part of this study area (see Figure 1a for location) was analyzed. The clay minerals in both the ZZ04 and DLC70-2 cores were within the range of sediments from the YR, the Shandong Peninsula rivers, and, in part, the Yangtze River. The influence of the Yangtze River may be attributed to the YSWC, which transports sediments from the south.

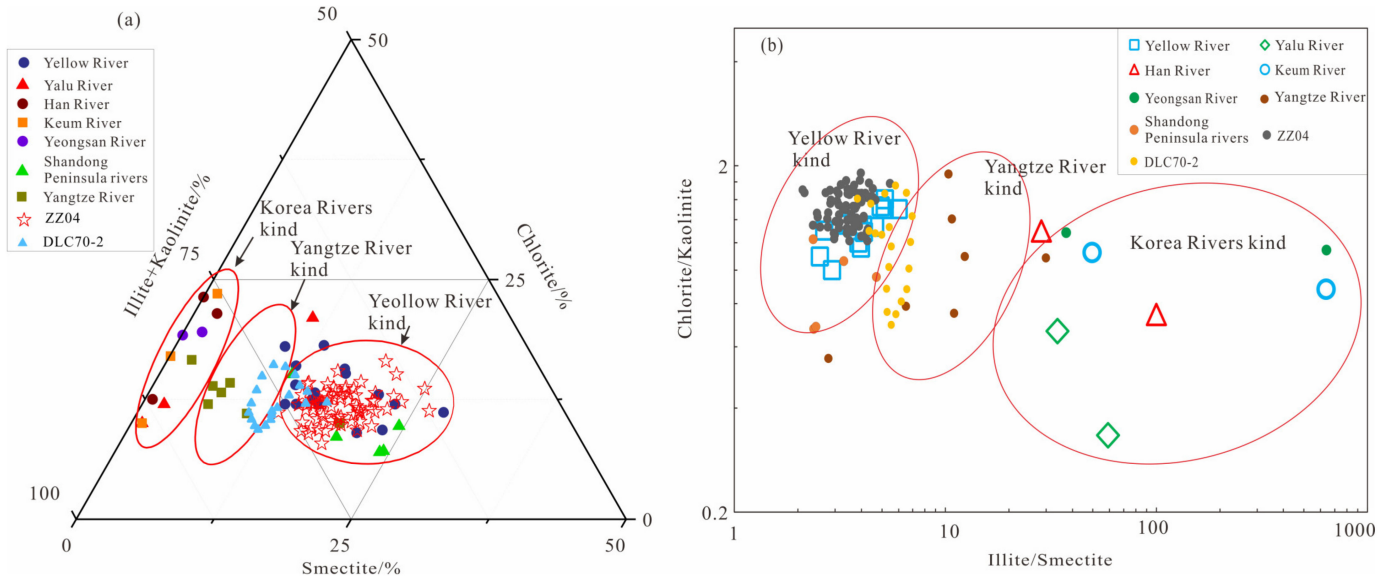

Figure 7. Cluster analysis of clay minerals in the cores of ZZ04 and DLC70-2, as well as river sediments around the NYS. (**a**) Ternary diagram of Smectite–chlorite–illite + kaolinite. (**b**) Crossplot of illite/smectite and chlorite/kaolinite.

5.2. Climate Change in the Mud Area over the Last 2000 Years

The formation of clay minerals is influenced by various factors, including river flows, warm currents, coastal currents, and climate. Generally, higher illite and chlorite levels suggest intensified physical weathering, meaning a drier and colder climate, whereas higher smectite and kaolinite levels indicate intensified chemical weathering, implying a warmer and more humid climate. A previous study has established that an increasing smectite/(illite + chlorite) ratio correlates with a warming climate trend [25,39].

In this study, we made a specific attempt to analyze the paleoclimate dynamics in China relative to global patterns, taking into account the influence of the EAM history. Our research extended to assessing the EAM's influence on the sediment sources within the NYS, including an evaluation of the terrestrial sources and the marine productivity. A comprehensive comparative analysis of the smectite/(illite + chlorite), Sr/Ca, and MgO/Al_2O_3 ratios in the ZZ04 core and the $\delta^{18}O$ data from the Dunde ice core [68], the Greenland GISP2 ice core [69], and Hongyuan peat [70] over the past 2000 years is presented in Figure 8. The climatic index, smectite/(illite + chlorite) ratio, was negatively correlated with both the Sr/Ca ratio and the Dunde ice core $\delta^{18}O$ values (proxy index of the East Asian winter monsoon; EAWM) [68]. This suggests that the smectite/ (illite + chlorite) ratio serves as a proxy for the East Asian summer monsoon (EASM) in the NYS. By analyzing the variations in these indicators, we identified four distinct climate change phases over the last 2000 years. They are discussed below in detail.

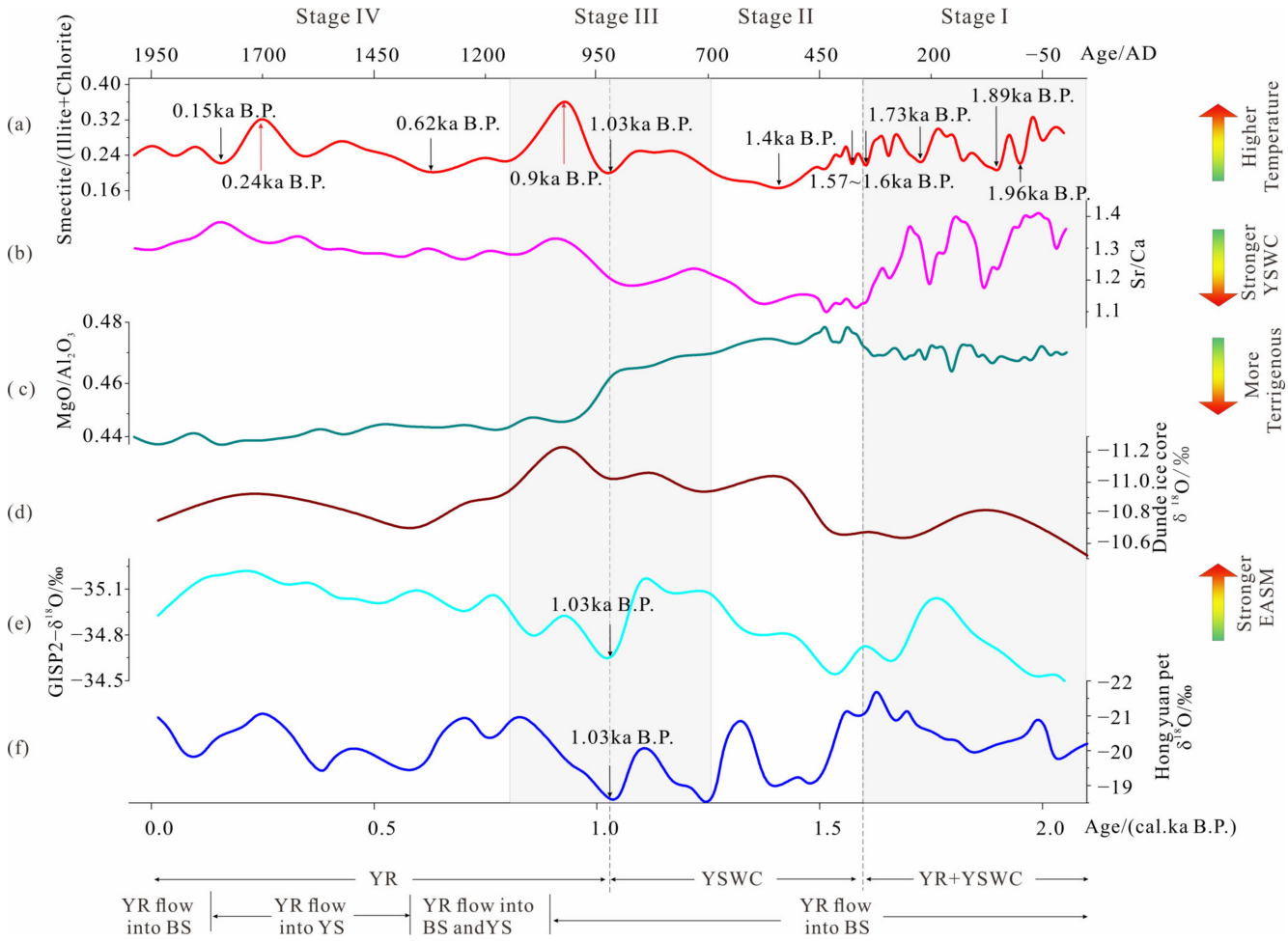

Figure 8. Comparison of clay mineral and geochemical element ratios in core ZZ04 sample with EAM curves over the past 2000 years. (**a**) The smectite/(illite + chlorite) ratio of the core ZZ04, (**b**) the Sr/Ca ratio of core ZZ04, (**c**) the MgO/Al_2O_3 ratios of the core ZZ04, (**d**) the $\delta^{18}O$ record of the Dunde ice core [68], (**e**) the $\delta^{18}O$ record of the GISP2 ice core from Greenland [69], and (**f**) the $\delta^{18}O$ record of the Hongyuan peat [70].

Stage I (2–1.6 cal.ka B.P.), characterized by moderate-to-high-frequency temperature fluctuations, aligns with the late Western Han Dynasty to the early Eastern Jin Dynasty in Chinese history (−50 to 350 AD) (Figure 8a). The climate during this period was marked by fluctuating intensities of the EAWM and EASM, with three notable cooling events at 1.96, 1.89, and 1.73 cal.ka B.P. These events correspond to the EAWM intensification periods from 2.2 cal.ka B.P. to 1.9 cal.ka B.P. and 1.7 cal.ka B.P. (Figure 8a), as suggested by Zhu et al. [71], and 1.88 cal.ka B.P., as suggested by Xiao et al. [72]. The grain-size of sediments in Stage I gradually became finer over time (Figure 2b,d). In terms of the clay mineral composition, the chlorite levels diminished, whereas kaolinite levels had a more pronounced variation (Figure 5c,d). Physical weathering predominantly occurred, although temperatures fluctuated. During the EAWM, sediments were predominantly sourced from the YR, with fine sands transported to the study area via the Bohai and Shandong coastal currents. Conversely, during the EASM, sediments were mainly sourced from the Shandong Peninsula rivers, contributing terrigenous materials shaped by chemical weathering processes.

Stage II (1.6–1.3 cal.ka B.P.) marks a cooling period that aligns with the low-temperature era of the Southern and Northern Dynasties in Chinese history (350–540 AD) (Figure 8a) [73,74]. This stage was characterized by the prevalence of the EAWM. A minor ice age occurred between 1.6 and 1.57 cal.ka B.P., followed by a significant cooling event at 1.4 cal.ka B.P.

(Figure 8a), which corresponds to the 1.4 cal.ka B.P. ice floe event in the North Atlantic [75]. Sediment grain-size analysis indicates a gradual increase in silt content and a corresponding decrease in clay content (Figure 2c,d). In terms of the clay mineral composition, there was a notable rise in illite content but a decline in smectite and chlorite contents (Figure 5a,c), indicative of a cold and dry climate. A high MgO/Al_2O_3 ratio and a low Sr/Ca ratio (Figure 8b,c) suggest a lower terrigenous input and higher marine productivity, respectively. The primary source of sediment during this period was the Yangtze River, with the YSWC facilitating the transport and deposition of sediments in the study area.

Stage III (1.3–0.8 cal.ka B.P.) represents a warming period in Chinese history, spanning from the Sui and Tang Dynasties (581–907 AD) to the Southern Song and Yuan Dynasties (1127–1320 AD). A brief cooling event occurred during the Five Dynasties to the Northern Song Dynasty (907–1127 AD) (Figure 8a) [73], during which the sediment's silt content continued to rise, whereas the clay content diminished (Figure 2c,d). The clay mineral composition showed a decrease in illite content and increases in the smectite and kaolinite contents (Figure 5b,d), signaling a significant paleoclimatic warming. Extreme weather events, i.e., a cold event at 1.03 cal.ka B.P. and a hot event at 0.9 cal.ka B.P., were recorded (Figure 8a). These cold events align with the Little Ice Age, as documented in the Dunde ice core [68], the GISP2 ice core [69], and Hongyuan peat [70] (Figure 8d–f). From 1128 AD, the YR's course was altered, flowing into both the BS and YS until 1494 AD, after which it exclusively flowed into the YS from Yancheng City, Jiangsu province, until 1579 AD [76]. After the cold event at 1.03 cal.ka B.P., there was a decline in the MgO/Al_2O_3 ratio and an increase in the Sr/Ca ratio (Figure 8b,c), indicating an intensification of the terrigenous material influx, which may be associated with the YR's course change. In Stage III, the EAWM's influence waned, whereas that of the EASM was strengthened (Figure 8a). At the beginning of this stage, the Yangtze River sediments, which were carried by the YSWC, were the main source significantly affecting the study area. As the EAWM weakened, the EASM became dominant, and the study area became increasingly influenced by the Shandong Peninsula rivers. During the warming climate, heavy precipitation events led to a decrease in the illite content and an increase in the smectite content, which is attributed to the leaching of potassium from illite and its subsequent transformation into smectite. This period concluded with a temperature decline at the end of the Yuan Dynasty.

Lastly, Stage IV (0.8 cal.ka B.P. to present), which was characterized by a stable cooler climate with a strengthened EAWM, coincided with the Little Ice Age and corresponded with the cold period during the Ming and Qing Dynasties in China (1321–1920 AD) [73,74] (Figure 8a). This stage included two Little Ice Age events at 0.62 cal.ka B.P. and 0.15 cal.ka B.P. The 0.62 cal.ka B.P. (Figure 8a), which was consistent with the climate events recorded in the Dunde ice core (1420–1520 AD) [77] and Hongyuan peat (1370–1400 AD) [70] (Figure 8d,f). The lithological trend of increasing silt content and decreasing clay content continued from the previous stages (Figure 2c,d). Additionally, decreases in chlorite and kaolinite contents (Figure 5c,d) reflected the predominantly cold climate. During this period, the MgO/Al_2O_3 ratio reached its minimum (Figure 8c), whereas the Sr/Ca ratio peaked at its maximum (Figure 8b), signifying the predominant influence of terrigenous material sources. The significant strengthening of the EAWM and the changes in the YR's course led to old YR-derived terrigenous clastic sediments, transported by the YSWC, becoming the primary source. The YR returned to the BS until 1855 AD, with minimal changes observed.

6. Conclusions

The main conclusions of this study are as follows:

(1) The ZZ04 core sample, acquired from the mud area in the northern offshore area of the Shandong Peninsula, predominantly consists of silt. The clay mineral composition is an assemblage of illite–smectite–chlorite–kaolinite. Illite, enriched with Fe-Mg, suggests strong physical weathering. Comparative analysis of the clay mineral composition of samples from the surrounding rivers, along with ternary diagram

and crossplot analyses, confirm that the sample's clay minerals are mainly sourced from the YR, the Shandong Peninsula rivers, and the Yangtze River, highlighting the multi-source characteristics of the sediments.

(2) The formation of the mud area was influenced by shifts in the East Asian monsoon, alterations in the YR's course, and dynamics of the YSWC. During the EAWM period, the coastal current's deposition rate and transport capacity led to a proportional increase in the terrigenous material input. Meanwhile, the YSWC was an important contributor in the transportation of matter and heat flux from the south. During the EASM period, sediments were mainly sourced from the Shandong Peninsula rivers, contributing terrigenous materials shaped by chemical weathering.

Author Contributions: Writing—original draft preparation, S.W.; supervision and writing, J.L.; generating the original data and performing the analytic calculations, Y.F. All authors have read and agreed to the published version of the manuscript.

Funding: This research was jointly funded by the Science and Technology Innovation Fund of the Command Center of Natural Resources Comprehensive Survey entitled "Temporal and spatial distribution of palaeochannel and origin of organic carbon burial in the Western Bohai sea since 2.28 Ma" (grant number KC20220011), the project entitled "Characterization of Carboniferous-Early Permian heterogeneous porous carbonate reservoirs and hydrocarbon potential analysis in the central uplift of the South Yellow Sea Basin" (grant number KLSG2304) funded by the Key Laboratory of Submarine Science, Ministry of Natural Resources, and the project entitled "1:25000 Marine Regional Geological Survey in Weihai Sea Area, North Yellow Sea (grant number DD20230412)", supported by the China Geological Survey.

Institutional Review Board Statement: Not applicable.

Informed Consent Statement: Not applicable.

Data Availability Statement: All the data and materials used in this paper are available from the corresponding authors upon request.

Acknowledgments: The authors would like to express their gratitude to the Yantai Center of Coastal Zone Geological Survey, China Geological Survey for providing the basic data and the Ph.D. students Jian Liu and X. Kong from the Qingdao Institute of Marine Geology for their help in this study. The authors are also grateful to the editors and reviewers who provided sincere comments and assisted in the writing of this manuscript. We are deeply grateful for the valuable suggestions provided by the three anonymous reviewers and the editorial assistance by the editors.

Conflicts of Interest: The authors declare no conflicts of interest.

References

1. Lv, W.Z. Sedimentary Processes and Mechanism of the Mud Areas on the China Sea Continental Shelf during the Middle to Late Holocene. Ph.D. Thesis, East China Normal University, Shanghai, China, 2022.
2. Liu, J.G.; Li, A.C.; Chen, M.H. Environmental evolution and impact of the Yellow River sediments on deposition in the Bohai Sea during the last deglaciation. *J. Asian Earth Sci.* **2010**, *38*, 26–33. [CrossRef]
3. Milliman, J.D.; Qin, Y.-S.; Ren, M.; Saito, Y. Man's influence on the erosion and transport of sediment by Asian rivers; the Yellow River (Huanghe) example. *J. Geol.* **1987**, *95*, 751–762. Available online: https://www.jstor.org/stable/30063822 (accessed on 2 August 2024). [CrossRef]
4. Liu, J.P.; Milliman, J.D.; Gao, S. The Shandong mud wedge and post-glacial sediment accumulation in the Yellow Sea. *Geo-Mar. Lett.* **2001**, *21*, 253–254. [CrossRef]
5. Liu, J.; Saito, Y.; Wang, H.; Yang, Z.G.; Nakashima, R. Sedimentary evolution of the Holocene subaqueous clinoform off the Shandong Peninsula in the Yellow Sea. *Mar. Geol.* **2007**, *236*, 165–187. [CrossRef]
6. Xue, C.T.; Qin, Y.C.; Ye, S.Y.; Laws, E.A.; Wang, Z.B. Evolution of Holocene ebb-tidal clinoform off the Shandong Peninsula on East China Sea shelf. *Earth-Sci. Rev.* **2018**, *177*, 478–496. [CrossRef]
7. Park, S.C.; Lee, H.H.; Han, H.S.; Lee, G.H.; Kim, D.C.; Yoo, D.G. Evolution of late Quaternary mud deposits and recent sediment budget in the southeastern Yellow Sea. *Mar. Geol.* **2000**, *170*, 271–288. [CrossRef]
8. Yang, Z.S.; Liu, J.P. A unique Yellow River-derived distal subaqueous delta in the Yellow Sea. *Mar. Geol.* **2007**, *240*, 169–176. [CrossRef]

9. Qiu, J.D.; Liu, J.; Saito, Y.; Yang, Z.G.; Yue, B.J.; Wang, H.; Kong, X.H. Sedimentary evolution of the Holocene subaqueous clinoform off the southern Shandong Peninsula in the Western South Yellow Sea. *J. Ocean Univ. China* **2014**, *13*, 747–760. [CrossRef]
10. Milliman, J.D.; Huang-Ting, S.; Zuo-Sheng, Y.; Meade, R.H.; Milliman, J.D.; Jin, Q. Transport and deposition of river sediment in the Changjiang Estuary and adjacent continental shelf. *Cont. Shelf Res.* **1985**, *4*, 37–44. [CrossRef]
11. Liu, J.P.; Li, A.C.; Xu, K.H.; Velozzi, D.M.; Yang, Z.S.; Milliman, J.D.; De Master, D.J. Sedimentary features of the Yangtze River-derived along-shelf clinoform deposit in the East China Sea. *Cont. Shelf Res.* **2006**, *26*, 2141–2156. [CrossRef]
12. Xiang, R.; Yang, Z.S.; Saito, Y.; Guo, Z.G.; Fan, D.J.; Li, Y.H.; Xiao, S.B.; Shi, X.F.; Chen, M.H. East Asia Winter Monsoon changes inferred from environmentally sensitive grain-size component records during the last 2300 years in mud area southwest off Cheju Island, ECS. *Sci. China Ser. D* **2006**, *49*, 604–614. [CrossRef]
13. Li, G.; Miao, L.; Yan, W. Holocene evolution of the shelf mud deposits in the north-western South China Sea. *Front. Mar. Sci.* **2022**, *9*, 937616. [CrossRef]
14. Alexander, C.R.; DeMaster, D.J.; Nittrouer, C.A. Sediment accumulation in a modern epicontinental-shelf setting; the Yellow Sea. *Mar. Geol.* **1991**, *98*, 51–72. [CrossRef]
15. Zhu, Y.T.; Xu, Y.C.; Liu, M.Y.; Lin, Z.B.; Zhu, L.H. Geochemistry and Holocene Sedimentary Environment Evolution of Subaqueous Clinoform off Shandong Peninsula (Yellow Sea). *Minerals* **2021**, *11*, 1209. [CrossRef]
16. Chang, X.; Liu, X.; Li, T.; Xiong, Z.; Duan, B.; Huang, J.; Liu, J.P.; Zhang, M.; Wang, A.; Wang, H. Late Quaternary marine transgressions off the Shandong Peninsula inferred from paleosalinity indicators: Implications for Holocene mud wedge formation. *Chem. Geol.* **2024**, *658*, 122117. [CrossRef]
17. Liu, J.P.; Milliman, J.D.; Gao, S.; Cheng, P. Holocene development of the Yellow River's subaqueous delta, North Yellow Sea. *Mar. Geol.* **2004**, *209*, 45–67. [CrossRef]
18. Wang, W.; Li, A.C.; Xu, F.J.; Huang, P.; Li, Y. Distribution of Surface Sediments and Sedimentary Environment in the North Yellow Sea. *Oceanol. Limnol. Sin.* **2009**, *40*, 525–531.
19. Chen, X.H.; Li, T.G.; Zhang, X.H.; Li, R.H. A Holocene Yalu River-derived fine-grained deposit in the southeast coastal area of the liaodong Peninsula. *Chin. J. Oceanol. Limnol.* **2013**, *31*, 636–647. [CrossRef]
20. Qi, J.; Li, F.Y.; Song, J.M.; Gao, S.; Wang, G.Z.; Peng, C. Sedimentation rate and flux of the North Yellow Sea. *Mar. Geol. Quat. Geol.* **2004**, *24*, 9–14.
21. Liu, J.; Saito, Y.; Kong, X.; Wang, H.; Zhao, L. Geochemical characteristics of sediment as indicators of post-glacial environmental changes off the Shandong Peninsula in the Yellow Sea. *Cont. Shelf Res.* **2009**, *29*, 846–855. [CrossRef]
22. Lan, X.H.; Mi, B.B.; Chen, X.H.; Li, R.H.; Wang, Z.B.; Lu, K. Tracing of Rare Elements in Late Quanternary Sediments from Central North Yellow Sea. *J. Chin. Soc. Rare Earths* **2015**, *33*, 241–252.
23. Han, Z.; Wang, Y.; Sun, Y.; Ai, X.; Wu, X.; Yang, Y. Composition of minerals in surface sediments of the Yellow Sea and their provenance. *Mar. Geol. Front.* **2022**, *38*, 10–19.
24. Dou, Y.G.; Li, J.; Zhao, J.T.; Wei, H.L.; Yang, S.Y.; Bai, F.L.; Zhang, D.L.; Ding, X.; Wang, L.B. Clay mineral distributions in surface sediments of the Liaodong Bay, Bohai Sea and surrounding river sediments: Sources and transport patterns. *Cont. Shelf Res.* **2014**, *73*, 72–82. [CrossRef]
25. Guo, R.S.; He, L.; Ye, S.Y.; Zhao, L.H. Mineral Characteristics, Provenance and Climatic Significance of Wetland Sediments from Dalinghe River Estuary in Liaohe Delta Since Late Pleistocene. *Geoscience* **2020**, *34*, 154–165.
26. Yang, S.X.; Ye, S.Y.; He, L.; Yuan, H.M.; Zhao, G.M.; Ding, X.G.; Pei, S.F.; Lu, J.F. Geochemical and clay mineral characteristics of the Holocene sediments on the west coast of Bohai Bay and their implications for environmental and climatic changes. *Mar. Geol. Quat. Geol.* **2021**, *41*, 75–87.
27. Xu, D.Y.; Liu, X.Q.; Zhang, X.H.; Li, T.G.; Chen, B.Y. *Offshore Geology of China*; Geological Publishing House: Beijing, China, 1997; p. 8.
28. Qin, Y.S.; Zhao, Y.Y.; Chen, L.R. *Geology of Yellow Sea*; Maritime Press: Beijing, China, 1989; p. 249.
29. Wu, S.Y.; Liu, J.; Chen, J.W.; Wu, H.R. Characteristics of Milankovitch cycles recorded in Eocene strata in the eastern depression of North Yellow Sea Basin, North China. *China Geol.* **2021**, *4*, 274–287. [CrossRef]
30. Shi, X.F. *China Offshore Oceanography-Seabed Matter*; Maritime Press: Beijing, China, 2016; pp. 25–139.
31. Guan, B.X. Patterns and Structures of the Currents in Bohai, Huanghai and East China Seas. *Oceanol. China Seas.* **1994**, *1*, 17–26.
32. Kim, K.H. Geochemical Study of Some Mesozoic Granitic Rocks in South Korea. *J. Korean Inst. Mining Geol.* **1992**, *25*, 435–446.
33. Hu, D.X. Upwelling and sedimentation dynamics. *China J. Oceanol. Limnol.* **1984**, *2*, 12–19.
34. Southon, J.; Kashgarian, M.; Fontugne, M.; Metivier, B.; Yim, W.W. Marine reservoir corrections for the Indian Ocean and southeast Asia. *Radiocarbon* **2002**, *44*, 167–180. [CrossRef]
35. Reimer, P.J.; Bard, E.; Bayliss, A.; Beck, J.W.; Blackwell, P.G.; Ramsey, C.B.; Buck, C.E.; Cheng, H.; Lawrence, E.R.; Michael, F.; et al. IntCal13 and Marine13 Radiocarbon Age Calibration Curves 0–50,000 Years cal BP. *Radiocarbon* **2013**, *55*, 1869–1887. [CrossRef]
36. Folk, R.L. The Distinction between Grain-size and Mineral Composition in Sedimentary-Rock Nomenclature. *J. Geol.* **1954**, *62*, 344–359. [CrossRef]
37. Biscaye, P.E.; Eittreim, S.L. Suspended particulate loads and transports in the nepheloid layer of the abyssal Atlantic Ocean. *Mar. Geol.* **1977**, *23*, 155–172. [CrossRef]
38. Ehrmann, W. Implications of late Eocene to early Miocene clay mineral assemblages in McMurdo Sound (Ross Sea, Antarctica) on paleoclimate and ice dynamics. *Palaeogeogr. Palaeoclimatol. Palaeoecol.* **1998**, *139*, 213–231. [CrossRef]

39. Liu, Z.F.; Trentesaux, A.; Clemens, S.C.; Colin, C.; Wang, P.X.; Huang, B.Q.; Boulay, S. Clay mineral assemblages in the northern South China Sea: Implications for East Asian monsoon evolution over the past 2 million years. *Mar. Geol.* **2003**, *201*, 133–146. [CrossRef]
40. Esquevin, J. Influence De La Composition Chimique Des Illites Sur Leur Cristallinite. *Bull. Cent. Rech. Pau-SNPA* **1969**, *3*, 147–153.
41. Gingele, F.X. Holocene climatic optimum in Southwest Africa—Evidence from the marine clay mineral record. *Palaeogeogr. Palaeoclimatol. Palaeoecol.* **1996**, *122*, 77–87. [CrossRef]
42. Liu, Z.F.; Tuo, S.T.; Colin, C.; Liu, J.T.; Huang, C.Y.; Selvaraj, K.; Chen, C.A.; Zhao, Y.L.; Siringan, F.P.; Boulay, S.; et al. Detrital fine-grained sediment contribution from Taiwan to the northern South China Sea and its relation to regional ocean circulation. *Mar. Geol.* **2008**, *255*, 149–155. [CrossRef]
43. Liu, S.F.; Shi, X.F.; Liu, Y.G.; Wu, Y.H.; Qiao, S.Q.; Yang, G. Recent 2000 a climatic record of mud area on the inner shelf of the East China Sea. *Acta Oceanol. Sin.* **2011**, *33*, 85–93.
44. Lund, B.; Ma, J. A review of cluster analysis techniques and their uses in library and information science research: K-means and k-medoids clustering. *Perform. Meas. Metr.* **2021**, *22*, 161–173. [CrossRef]
45. Stoll, H.M.; Schrag, D.P. Coccolith Sr/Ca as a new indicator of coccolithophorid calcification and growth rate. *Geochem. Geophys. Geosystems* **2000**, *1*, 1006. [CrossRef]
46. Li, Y.; Li, A.C.; Huang, P.; Xu, F.J.; Zheng, X.F. Clay minerals in surface sediment of the north Yellow Sea and their implication to provenance and transportation. *Cont. Shelf Res.* **2014**, *90*, 33–40. [CrossRef]
47. Liu, J.Q.; Liu, Y.L.; Yin, P.; Gao, F.; Cao, K.; Chen, X.Y. Composition, Source and Environmental Indication of Clay Minerals in Sediments from Mud Deposits in he Southern Weihai Offshore, Northwestern Shelf of the South Yellow Sea, China. *J. Ocean Univ. China* **2022**, *21*, 1161–1173. [CrossRef]
48. Fan, D.J.; Yang, Z.S.; Mao, D.; Guo, Z.G. Clay Minerals and Geochemistry of the Sediments from the Yangtze and Yellow Rivers. *Mar. Geol. Quat. Geol.* **2001**, *21*, 7–12.
49. Milliman, J.D.; Beardsley, R.C.; Zuo-Sheng, Y.; Limeburner, R. Modem Huanghe-derived muds on the outer shelf of the East China Sea: Identification and potential transport mechanisms. *Conitinental Shelf Res.* **1985**, *4*, 175–188. [CrossRef]
50. Xu, K.H.; Milliman, J.D.; Li, A.C.; Liu, J.P.; Kao, S.J.; Wan, S.M. Yangtze and Taiwan derived sediments on the inner shelf of East China Sea. *Cont. Shelf Res.* **2009**, *29*, 2240–2256. [CrossRef]
51. Xu, D.Y. Mud sedimentation on the east China sea continental shelf. *Mar. Geol. Quat. Geol.* **1985**, *5*, 17–26.
52. Ren, M.; Shi, Y. Sediment discharge of the Yellow River (China) and its effect on the sedimentation of the Bohai and the Yellow Sea. *Cont. Shelf Res.* **1986**, *6*, 785–810. [CrossRef]
53. Yang, Z.S. Mineralogical assemblages and chemical characteristics of clays from sediments of the huanghe, changjiang, zhujiang rivers and their relationship to the climate environment in their sediment source areas. *Oceanol. Limnol. Sin.* **1988**, *19*, 336–346.
54. Yang, S.Y.; Jung, H.S.; Lim, D.I.; Li, C.X. A review on the provenance discrimination of sediments in the Yellow Sea. *Earth-Sci. Rev.* **2003**, *63*, 93–120. [CrossRef]
55. He, M.Y.; Zheng, H.B.; Huang, X.T.; Jia, J.T.; Li, L. Yangtze River sediments from source to sink traced with clay mineralogy. *J. Asian Earth Sci.* **2013**, *69*, 60–69. [CrossRef]
56. Xu, D.Y. Mud sedimentation on the East China Sea shelf. In Proceedings of the International Symposium on Sedimentation on the Continental Shelf with Special Reference to the East China Sea, Hangzhou, China, 12–16 April 1983.
57. Lu, J.; Li, A.C.; Huang, P.; Li, Y. Mineral distributions in surface sediments of the western South Yellow Sea: Implications for sediment provenance and transportation. *Chin. J. Oceanol. Limnol.* **2015**, *33*, 510–524. [CrossRef]
58. Hu, G.; Xu, K.; Clift, P.D.; Zhang, Y.; Li, Y.; Qiu, J.; Kong, X.; Bi, S. Textures, provenances and structures of sediment in the inner shelf south of Shandong Peninsula, western South Yellow Sea. *Estuar. Coast. Shelf Sci.* **2018**, *212*, 153–163. [CrossRef]
59. Lan, X.H.; Zhang, X.J.; Liu, X.B.; Li, R.H.; Zhang, Z.X. Distribution pattern of clay minerals in surface sediments of South Yellow Sea and their provenance. *Mar. Geol. Quat. Geol.* **2011**, *31*, 11–16. [CrossRef]
60. Seo, K.W.; Chi, J.M.; Jang, Y.H. Geochemical relationship between shore sediments and near terrestrial geology in Byunsan-Taean area, west coast of korea. *Econ. Environ. Geol.* **1998**, *31*, 69–84. Available online: https://koreascience.kr/article/JAKO199823034627177.do (accessed on 2 August 2024).
61. Yang, S.Y.; Li, C.X.; Lee, C.B. Rare earth element geochemistry and sediment source tracing in rivers around the Yellow Sea. *Chin. Sci. Bull.* **2003**, *48*, 1233–1236. [CrossRef]
62. Park, C.K.; Oh, J.K. A Study on the Clay Minerals in the Han River Estuary and the Kyonggi Bay Areas. *J. Korea Soc. Oceanogr.* **1991**, *26*, 313–323. Available online: https://koreascience.kr/article/JAKO199111920647699.do (accessed on 2 August 2024).
63. Park, Y.A.; Khim, B.K. Origin and dispersal of Recent clay minerals in the Yellow Sea. *Mar. Geol.* **1992**, *104*, 205–213. [CrossRef]
64. Cho, H.G.; Kim, S.; Kwak, K.Y.; Choi, H.; Khim, B. Clay mineral distribution and provenance in the Heuksan mud belt, Yellow Sea. *Geo-Mar. Lett.* **2015**, *35*, 411–419. [CrossRef]
65. Choi, J.H. Recent Clay Minerals in the Kunsan Estuary and the Adjacent Continental Shelf. Master's Thesis, Seoul National University, Seoul, Republic of Korea, 1981.
66. Kim, D.C. Recent Clay Minerals of the Yeongsan Estuary and the Adjacent Continental Shelf. Master's Thesis, Seoul National University, Seoul, Republic of Korea, 1980.
67. Gao, J.H.; Li, J.; Wang, Y.P.; Bai, F.L.; Li, J.S.; Cheng, Y. Heavy mineral distributions and their implications for sediment dynamics in the Yalu Estuary and its adjacent sea area. *Acta Oceanol. Sin.* **2009**, *31*, 84–94.

68. Shi, Y.F.; Kong, Z.C.; Wang, S.M.; Tang, L.Y.; Wang, F.B.; Yao, C.D.; Zhao, X.T.; Zhang, P.Y.; Shi, S.H. Climatic fluctuations and important events during the Holocene Great Warm Period in China. *Sci. China Ser. B* **1992**, *12*, 1300–1308.
69. Stuiver, M.; Grootes, P.M.; Braziunas, T.F. The GISP2 δ18O climate record of the past 16,500 years and the role of the sun, ocean, and volcanoes. *Quaternary Res.* **1995**, *44*, 341–354. [CrossRef]
70. Xu, H.; Hong, Y.T.; Lin, Q.H.; Hong, B.; Jiang, H.B. Temperature changes from 6ka to present as indicated by oxygen isotope of cellulose in Hongyuan Peat. *Chin. Sci. Bull.* **2002**, *47*, 1181–1186.
71. Zhu, Y.M.; Tian, Y.; Yin, P.; Duan, X.Y.; Cao, K.; Liu, D.Y. Response of high-resolution sedimentary records to East Asian winter monsoon in the inner shelf of the East China Sea over the past 8000 years. *Mar. Geol. Front.* **2023**, *39*, 1–10.
72. Xiao, S.B.; Li, A.C.; Chen, M.H.; Liu, J.P.; Jiang, F.Q. Recent 8ka Mud Records of the East Asian Winter Monsoon from the Inner Shel of the East China Sea. *Earth Sci. J. China Univ. Geosci.* **2005**, *30*, 573–581.
73. Ge, Q.S.; Zhu, H.Y. Changes of the physical and human geographical environment in China during the past 2000 years. *Acta Geogr. Sin.* **2021**, *76*, 3–14.
74. Ge, Q.S.; Fang, X.Q.; Zheng, J.Y. Learning from the historical impacts of climatic change in China. *Adv. Earth Sci.* **2014**, *29*, 23–29.
75. Bond, G.; Showers, W.J.; Cheseby, M.; Lotti, R.; Almasi, P.; DeMenocal, P.; Priore, P.; Cullen, H.; Hajdas, I.; Bonani, G. A pervasive millennial-scale cycle in North Atlantic Holocene and glacial climates. *Science* **1997**, *278*, 1257–1266. [CrossRef]
76. Xue, C.T.; Liu, J.; Kong, X.H. Channel shifting of lower Yellow River in 1128-1855AD and its influence to the sedimentation in Bohai, Yellow and east China Seas. *Mar. Geol. Quat. Geol.* **2011**, *31*, 25–36. [CrossRef]
77. Yao, C.D.; Xie, Z.C.; Wu, X.L.; Thompson, L.G. Little Ice Age climate records in the Dunde Ice Cap. *Sci. China Ser. B* **1990**, *11*, 1196–1201.